ISTITUTO NAZIONALE FISICA NUCLEARE

INFN/AE - 84/9
8 settembre 1984

C. Cernigoi, R. Cherubini, N. Grion, G. Pauli
and R. Rui:

NEUTRONS, PROTONS, AND DEUTERONS EMITTED AFTER ABSORPTION OF STOPPED π^- IN ^{6}LI, ^{9}BE, ^{16}O AND ^{27}AL

SERVIZIO RIPRODUZIONE DELLA
SEZIONE DI TRIESTE DELL'INFN

NEUTRONS, PROTONS, AND DEUTERONS EMITTED AFTER ABSORPTION OF STOPPED NEGATIVE PIONS IN ^{6}Li, ^{9}Be, ^{16}O AND ^{27}Al

C. CERNIGOI, N. GRION (*), G. PAULI and R. RUI

Istituto di Fisica, Universita' degli Studi , Trieste

and

INFN, Sezione di Trieste, Italy

and

R. CHERUBINI

Istituto di Fisica, Universita' degli Studi , Padova

and

INFN, Laboratori di Legnaro, Padova, Italy

(*) Present address: TRIUMF, Vancouver, Canada

CONTENTS

1.0 INTRODUCTION

The measurement of inclusive energy spectra of highly energetic ($E \geq 20$ MeV) neutrons, protons and deuterons emitted after the absorption of stopped negative pions in light nuclei is an useful tool for investigating the pion absorption process [1-8]. This process is described in terms of either the two-nucleon [3] or the many-nucleon [4] absorption mechanism. Measurements of the high-energy parts of neutron and proton spectra can provide indications about the competition between these two mechanisms, since in these regions final state interactions (FSI) weakly affect the information brought by nucleons directly involved in the absorption process (primary nucleons).

Another problem concerns the single-nucleon emission process [5,6] which can be investigated by accurate measurements of the highest energy end of the nucleon spectra.

Finally, energy measurements of the highly energetic deuterons can give information as to whether such particles are emitted after many-nucleon absorption of pions (and are then "pre-existing" in the nucleus) or whether they are emitted as a result of two-nucleon absorption followed by FSI (pick-up or knock-out reactions) [7,8].

The present report gives the results of an experiment conducted with the aim of measuring neutron, proton and deuteron spectra from ^{6}Li, ^{9}Be, ^{16}O and ^{27}Al (only neutrons). Measurements were performed with good energy resolution, such that in the neutron spectra of all the studied nuclei clear evidence was obtained of structures kinematically corresponding to the emission of a single neutron.

Inclusive energy spectra of neutrons were measured for ^{6}Li by Bassalleck et al. [9] and by Isaak et al. [12], for ^{9}Be by Bassalleck et al. [9], for ^{16}O by Klein et al. [10] and by Madey et al. [11], and for ^{27}Al by Madey et al. [11]. Inclusive proton and deuteron spectra were measured for ^{6}Li by Sennhauser et al. [13]

2.0 EXPERIMENTAL PROCEDURE

2.1 Pion Beam Monitor

The experiment was carried out using the M11 and M13 beam lines at TRIUMF. Particles furnished by these channels were monitored by a beam telescope (BT) of 6 plastic scintillator counters placed, with respect to the pion beam direction, as shown in fig.1.

This BT, described in ref.14, is different from the conventional ones [9,10,12,13] since it includes two more vetocounters which facilitate a better determination of the absolute number of stopped pions.

All the incoming beam particles (π^-, μ^- and e^-) were identified by measuring their time-of-flight (TOF) between the T1 pion production target [15] and the plastic counter labelled CT2 in fig.1. To this purpose, a signal from a capacitive probe (CP) in the main proton beam line was used as stop signal, while the start signal was delivered by the CT2 counter.

An incident pion was monitored by the coincidence $I = CP*CM1*CT2*CM3*\overline{CA4}*\overline{CA6}$ and a stopped pion by the coincidence $S = CP*CM1*CT2*CM3*\overline{CA4}*\overline{CA5}*\overline{CA6}$. The ratio R = S/I determined the inefficiency of the CA5 counter. When only the electron beam component was selected R = 0.3%. The same value was obtained for vetocounters CA4 and CA6.

Fig.2 shows the range curve measured for ^{16}O (H_2O target) as a function of the CH_2 degrader thickness using M13 pions with initial energy of 43 MeV. Range curves for the other targets had the same behaviour as for ^{16}O and are not reported in the figure. The outstanding feature of such range curves is the high stopping rate in thin targets (see table 1). It is important to note that the doorway for both reliable background subtraction and absolute pion stop normalization is a high stopping rate together with a high target-in to target-out ratio. Relevant quantities related to the experiment are listed in table 1.

In the case of the M11 channel, a satisfactory compromise was obtained between the pion flux intensity and the degrader thickness needed to slow down the incoming pions when pions with initial energy of 90 MeV were chosen. However, the use of thicker targets (2 g/cm²) was necessary to assure significative statistics for the collected events (only neutrons) in a reasonable amount of time.

2.2 Absolute Number Of Stopped Pions

As described above, a stopped pion was monitored by a coincidence signal $CP*CM1*CT2*CM3*\overline{CA4}*\overline{CA5}*\overline{CA6}$. However, every particle passing through CM3 and missed by vetocounters simulated a stopped pion. When the selected degrader thickness was inserted, the largest source of such events were pions decaying into muons between CM3 and the target position. Other sources, like the BT inefficiency, did not sensibly contribute to the statistics, since they accounted for only a few per mill.

A slowed down pion merging from CM3 has an energy which was calculated to be 12 MeV, on the average. The probability for the pion to decay before being absorbed by a target nucleus is 6%. Within this probability, due to the "non--conventional" geometry of our BT, about 30% of the daughter muons are not vetoed. Thus, the total number of stopped pion coincidence signals is contaminated by (less than) 2%.

As stated above, the BT inefficiency was mainly due to daughter muons of lower energy coming from pion decays, specifically, muons of energy not greater than 2 MeV. In fact, a 2 MeV muon born at CM3 and travelling from CM3 to a vetocounter loses at most 0.5 MeV and reaches the vetocounter with about 1.5 MeV energy. Now, the beam electrons release 0.9 MeV in the vetocounters and 1.5 MeV muons have the same scintillation response as these electrons [16]. So the BT efficiency of 99.7% measured for beam electrons can be attributed to 2 MeV muons coming from pion decays. These muons, according to the kinematics of pion decay (full curve in fig.3) span an angle from 0 up to 34 degrees and the fraction of muons emitted in this angular range can be evaluated by integrating the dashed curve in fig.3 within the same angles. This curve illustrates the relative number of muons emitted after the decay of 12 MeV pions as a function of the lab angle; it was generated by exploiting the isotropy of pion decay in the center-of-mass frame. In our case the percentage of muons with an energy less than 2 MeV, emitted from 0 to 34 degrees, accounted for 29% of the total number of emitted muons.

The overall percentage of muons missed by vetocounters was determined by integrating over the pion energy range. Such a value turned out to be slightly lower than 29%.

2.3 Neutron Detection

Particles in coincidence with a stopped pion were detected by four bars of NE110 plastic scintillator $(200 \times 15 \times 5) cm^3$ [17-19]. Neutron signals were electronically picked out by vetoing charged particle signals with vetocounters CA4, CA5 and CA6 and by rejecting nuclear gamma signals with a safely high pulse threshold corresponding to 14 MeV proton energy. In fact, since this experiment proposed to measure the high energy region ($E \geq 20$ MeV) of the particles emitted after pion absorption, a high common neutron detection threshold (14 MeV) was chosen. The neutron efficiency was calculated with the Monte Carlo code of ref.20 and normalized to the experimental value at 90 MeV obtained by measuring the yield of monoenergetic neutrons of the $^4He(\pi^-,n)^3H$ reaction [21].

Neutron energies were measured with the TOF method over a flight distance of 510 cm for N1 and N2 and 480 cm for N3 and N4 (notations are referred to fig.1). The overall time resolution was of 650 psec at FWHM.

As an example, the neutron TOF spectrum measured for ^6Li is shown in fig.4. In this figure a prompt peak is evident, which is due to particles flying with the speed of light. These particles are mainly gammas produced by radiative pion captures or pion charge exchange reactions in proximity of the target. Indeed, electrons missed by vetocounters might also contribute to this peak. It is interesting to note that in the background spectrum the prompt peak is much broader. This is due to the fact that induced gammas do not originate in a fixed point (the target), but in an extended region surrounding the target (vetocounter, CM3, frames and air). In fact, after background subtraction, the prompt peak is sharply defined, clearly indicating the target contribution, and this was used for calibrating the time axis of the spectrum [22]. The part of the TOF spectrum corresponding to the highest energies is shown in fig.5. The contribution of particles in the kinematically forbidden region, corresponding to TOFs between 18 and 34 nsec, is ascribable to chance coincidences.

2.4 Charged Particles Detection

Protons and deuterons were mass identified by a range telescope (RT) described in ref.23. It consisted of an array of eight NE110 plastic scintillator slabs 20*80 cm^2 having different thicknesses. For every detected particle the three quantities β, approximate range and E*dE were measured. The two plots E*dE versus β and β versus range unambiguosly identified p and d from other detected charged particles. A charged event was definitevely rejected when only a dE signal (provided by the first slab of the RT) was recorded. This resulted in an energy threshold of 18 and 26 MeV for p and d, respectively. An E signal (provided by the other seven slabs of the RT) not followed by a dE signal identified "neutral" events. These events were mainly due to neutrons, since nuclear gammas were biased by the high neutron detection energy threshold, set at 12 MeV proton energy. The neutron efficiency was calculated with the method described in the previous paragraph.

Proton and deuteron energies were determined by measuring their TOFs over a flight path of 388 cm with an overall time resolution of 700 psec at FWHM.

2.5 Data Reduction And Analysis

The differential neutron and proton energy spectra, in units of events per stopped pion per MeV, were calculated with the following expression:

$$\frac{\text{EVENTS}}{\pi^{-}\text{-stop*MeV}} = \frac{4\pi}{\Omega} * \frac{A}{\pi^{-}\text{-stop*dE}}$$

where A is the number of counts in an interval E , E+dE, Ω is the total solid angle of the counters, π^{-}-stop is the absolute number of stopped pions, and dE is the binning energy interval (in units of MeV). For a given energy E, the quantity A was evaluated as $A = (B-\alpha C)/\varepsilon(E)$, where B are the events collected with target-in, C the events collected with target-out, α is a parameter defined below, and $\varepsilon(E)$ is the efficiency of the counter, being 1 in the case of charged particle detection. The absolute number of stopped pions was evaluated as $T - \alpha F$, where T and F are the total number of pions stopped with target-in and -out, respectively, and α is defined as

$$\alpha = \frac{T}{F} * \frac{f}{t} \quad .$$

where t and f are the numbers of pions stopped per second (100 μA primary beam) with target-in and target-out, respectively.

The neutron spectra obtained from five independent counters allowed us to check for possible systematic errors that would result in an incorrect behaviour of the final spectra. In fact, from this comparison data from the neutron counters N1 and N2 were rejected because they showed the beam time structure added up over the time of flight spectra. Moreover, having used one of the five counters (RT) for both neutron (n) and charged particle (ch) detection, and being both spectra measured simultaneously, we were confident that the values of the n/ch ratios evaluated from these data were accurate.

Vertical error bars in the neutron and charged particle spectra were calculated from the above expression by propagating the errors. Poisson statistics were used to evaluate errors for B and C. No error was assumed in the evaluation of the solid angle because of the small depth of the counters compared to the counter-to-target distance. Because of the very good discrimination between pions and other particles (muons and electrons) in the beam, and because of the high target-in to target-out ratio, the error in defining the absolute number of stopped pions in the target was relatively small compared to other errors. Finally, the error associated with the evaluation of ε(E) was ±5% as given by the authors of ref.20.

Particular accuracy was used to evaluate the yields for the single nucleon emission: both background due to chance coincidences and three body phase space contribution folded with the energy resolution were subtracted. The statistical error associated with the background was taken into account.

In the case of charged particle emission all the measured yields are given with an error that also includes a 6% error (upper limit) due to inefficiency in discriminating among charged particles.

Finally, the yield of neutron emission from the ^{16}O target was calculated for two different sets of data collected in different runs using two different beam channels (see table 1). Neutron intensities with M11 were 6% lower than those with M13 (quoted in this paper), while there was no appreciable difference in the shape of the two spectra. This discrepancy is most likely ascribable to muons from pion decays that were stopped by the thicker target, and to a large experimental background originated by the slowing down of the higher energy pions delivered by the M11 channel.

2.6 Energy Resolution

Horizontal error bars in the neutron energy spectra were determined from the time resolution of the system, while in the case of charged particle spectra the error due to energy loss in the target also contributed to the total error. Thin targets of 0.5 g/cm^2 thickness or less were used so that the error in the energy determination of protons and deuterons due to energy losses in the targets did not appreciably affect the energy resolution in the high energy region of the spectra. The overall time resolution of the system was assumed to be equal to the observed width (FWHM) of the prompt peak for the ^{6}Li target. The time resolution was 650 psec for counters N3 and N4, and 700 psec for the other counters (In the TOF spectrum of fig.5 it results larger because of the binning interval of 400 psec). The FWHM measured with the counters positioned downstream of the beam, and using the electron component of the beam, was found to be of 400-450 psec, thus confirming the calculated value of 530 psec for the time jitter of the pions going from the CT2 counter to the target.

3.0 EXPERIMENTAL RESULTS

3.1 Neutron Measurements

The measured energy spectra of neutrons emitted after absorption of stopped negative pions in ^{6}Li, ^{9}Be, ^{16}O and in ^{27}Al are shown in figs.6-9. The error in energy in all these spectra is about 4% at 110 MeV. All spectra are shown with background subtracted. The residual background from chance coincidences is indicated by dashed lines. The expected contributions of the $(\pi^-,2N)$ reactions to the inclusive neutron spectra were calculated with the three-body phase-space and are shown by the solid lines. These calculations were normalized to the measured spectra in the region delimited by the kinematical limits of three-body $(\pi^-,2N)$ and four-body $(\pi^-,3N)$ reaction channels. To carry out the normalization, the chance coincidence background was subtracted from the energy spectra.

<u>^{6}Li spectrum</u> (fig.6). A bump at about 110 MeV standing out above the continuous distribution of neutrons from the three-body $(\pi^-,2n)$ channel is a possible sign of the single neutron emission. On kinematical grounds, this bump can be attributed to the two body channel (π^-,n) leading to ^{5}He residual nucleus. In any case, even setting aside the energy resolution of our apparatus, one would not expect to see a peak since the ground state of ^{5}He appears to be a resonant state (^{4}He + n) + 1.15 MeV. By subtracting the three body phase-space contribution and the chance coincidence

background from the high-energy tail of the spectrum, one unfolds the area of the bump at 110 MeV that corresponds to a rate of $(1.31\pm0.29)\times10^{-2}$ neutrons per stopped pion.

The spectra measured by Bassalleck et al. [9] (histogram) and by Isaak et al. [12] (open triangles) are shown for comparison.

Both the present spectrum and that measured in ref.12 show a broad maximum centered around 65 MeV. It is accounted for by neutrons of the $^{6}Li(\pi^{-},2n)^{4}He$ reaction emitted with an opening angle close to 180°. In this case, neutrons carry away an energy $E = (1/2)*Q \approx 67$ MeV, where Q is the Q-value of the reaction. The present spectrum differs from the measurements of Isaak et al. in the 20-50 MeV region, where it is up to 50% higher, and above 90 MeV. The discrepancy in the region from 20 to 50 MeV can be attributed to different determinations of the neutron detection efficiency. As pointed out by K. Nakayama et al. [24] and Madey et al. [11], differences in either neutron detection threshold or code contribute to different determination of $\varepsilon(E)$. In ref.12 a Monte Carlo code based on the code of Del Guerra et al., therein quoted, was used and the threshold was set to 3 MeV neutron energy. In the present work a Monte Carlo code based on the Stanton code was used [20], with a neutron energy threshold of 12 MeV. As far as the discrepancy above 90 MeV is concerned, one notices in the spectra of Isaak et al. [12] that the energy resolution was of the order of 16% at 110 MeV - compared to 4% in the present measurement - so that possible structures were smeared out.

With respect to the measurement of Bassalleck et al. [9], which covers the energy region of 90-120 MeV with an energy resolution of 4 MeV, the present spectrum agrees in shape but is one order of magnitude higher in intensity. In fact, as reported in Table 2, Bassalleck et al. found a rate for the (π^-,n) reaction of $(1.6\pm0.8)\times10^{-3}$ neutrons per stopped pion, that is, smaller by a factor 10 than that found in the present measurement. The possible sources of this discrepancy were discussed in detail by the authors in ref.22.

<u>^{9}Be spectrum</u> (fig.7). The monotonically decreasing curve of the neutron spectrum with energy up to about 100 MeV does not point to any particular reaction channel. In this spectrum a shoulder is observed at 110 MeV which could represent a contribution from the (π^-,n) channel leading to the ground and excited states of ^{8}Li. For this channel a rate of $(2.46\pm0.40)*10^{-2}$ neutrons per stopped pion was unfolded from the experimental data. Bassalleck et al. [9] found a rate between 0 and $0.15*10^{-3}$ per stopped pion.

<u>^{16}O spectrum</u> (fig.8). In this case, although no clear structure is visible in the spectrum, a gaussian fit (with FWHM equal to the experimental energy resolution) to the final part of the spectrum permitted us to unfold a peak at an energy pertinent to neutrons emitted in the single-neutron emission process leading to the ground state of ^{15}N. Two attendant circumstances allowed such a

procedure: a) ^{15}N is stable and our energy resolution could resolve the g.s. of ^{15}N from its excited states, and b) both the $(\pi^-,2n)$ and the (π^-,np) channels open at about 10 MeV below the (π^-,n) threshold. For this process a rate of $(1.25\pm0.27)\times10^{-2}$ neutrons per stopped pion was deduced.

In fig.8 the present measurement is compared with that of Madey et al. [11] (open triangles). The spectrum measured by Klein et al. [10] closely follows that of Madey et al. and is not reported in the figure. The results of Madey et al. substantially agree with the present results above about 60 MeV, while from 20 to 60 MeV they are lower by 30%. In this case as well, the discrepancy below 60 MeV can be due to different codes and detection thresholds used for the determination of the neutron detection efficiency. As far as the high-energy part of the spectrum (>100 MeV) is concerned, it should be noted that the neutron spectra were measured with energy resolutions of 17-18% at 100 MeV by Madey et al., and 30% at 100 MeV by Klein et al.. For these authors the same problem of Isaak et al. [12] arises, namely, that possible structures in the high energy part of the spectrum could not be brought forth.

Oxygen data are also compared in fig.8 with the calculations of Chiang and Hüfner [3] for ^{12}C (dotted-dashed line) and by Jackson and Brenner [4] for oxygen/carbon (dotted line). The calculations of Chiang and Hüfner for ^{12}C, based on the two-nucleon absorption, reasonably reproduce the measured neutron spectrum for ^{16}O in the uncertanties, the result seems to be independent of the studied nucleus.

Our R_{np} values are also in agreement with theoretical calculations of the pion absorption process by Shimizu et al. [25]. In their predictions the p-wave π-NN interaction procedes through a Δ excitation in the intermediate state, and they calculate R_{np} = 7.2, 8.5, and 15.0 when the NN correlations are accounted for π , $\pi + \rho$ and $\pi + \rho + \pi\pi$ exchange, respectively.

Experimental ratios found in the literature (ref.2, for a rewiew, and refs.12,26) were not reported in table 4 together with our results because they were derived from yields covering different regions where protons are mainly secondary ones.

In Fig.12 the measured proton spectrum for ^{16}O is compared with the proton spectrum calculated for ^{12}C by Chiang and Hüfner [3]. The same observations made in connection with the neutron spectrum of ^{16}O hold for this comparison. The calculated spectrum for ^{12}C satisfactorily reproduces the measured spectrum for ^{16}O except below 60 MeV. In ref.3 the calculated spectrum reproduced experimental spectra for ^{12}C with R_{np} = 9.6.

The inclusive deuteron energy spectra of ^{9}Be and ^{16}O show no structure decreasing smoothly with increasing energy. This type of behaviour is predicted by calculations of Hachenberg et al. [7] of deuteron spectra in pion-induced pre-compound reactions, performed according to a model based on the idea that the observed deuterons can be explained by a two-nucleon absorption mechanism followed by a nucleonic cascade and pick-up in the outer regions of the nucleus. However, a peculiar feature is shown by the deuteron spectrum of ^{6}Li (fig.10) where there is an indication of a shoulder at an energy of about 75 MeV. This feature is also present in the deuteron spectrum of ^{6}Li, measured by Sennhauser et al. [13], and reported in fig.10 (open squares). The shoulder corresponds energetically to deuterons of the two-body reaction ^{6}Li$(\pi^-,d)^4$H. This reaction could be explained in terms of cluster absorption, where, in this case, the whole nucleus partecipates in an absorption process [13,27]. In the case of ^{6}Li the absorption would be followed by the break-up of ^{6}Li into a deuteron and a ^{4}H, where the ^{4}H decays into a triton and a neutron. Such a reaction could account for a partial contribution of tritons to the triton spectrum of ^{6}Li [13]. In fact, calculations performed by Hackenberg [29] show that the observed tritons produced in the pion-induced pre--compound reactions cannot be explained by assuming only a two-nucleon mechanism followed by the formation of composite particles by pickup, but that cluster absorption must also be admitted.

More refined calculations for the deuteron spectra, based on the same assumption of Hackenberg et al. [7] have been performed by Datar and Jain [8], who describe the final state interaction using the partial wave formalism of the

DWBA. In order to test the validity of these calculations, the predicted deuteron spectrum for ^{12}C, assuming a contribution from nucleons of the whole nuclear volume, is compared in Fig.12 (dashed curve) with the measured deuteron spectrum for ^{16}O. The same observations made in connection with the neutron spectrum of ^{16}O hold for this comparison. There is good qualitative agreement between the calculations and the measured spectrum, except that the magnitude is overestimated.

A calculation of the deuteron spectrum for ^{16}O was carried out by Jackson and Brenner [4] on the basis of the α-cluster absorption mechanism. These authors obtained a spectrum, not reported in fig.12, which is too steep compared to the present measured spectrum.

4.0 CONCLUSIONS

In this report a measurement of the energy spectra of neutrons, protons, and deuterons emitted following the absorption of stopped negative pions on ^{6}Li, ^{9}Be, ^{16}O, and ^{27}Al (only neutrons) was presented.

From the results of the measurement the following conclusions can be drawn.

Structures put in evidence in the high energy part of the neutron spectra were attributed to single neutron emission and the corresponding yields are reported in table 2.

The probability of single-neutron emission was calculated by Coupat et al. [6] in the framework of the two--nucleon absorption model, and by Troitskii et al [29] in that one of the single nucleon absorption model. In ref.6 a calculated probability of $2.5-2.8\times10^{-3}$ neutron per stopped pion for ^{12}C is reported. This value is one order of magnitude lower than the probabilities for ^{6}Li, ^{9}Be, and ^{16}O measured in our experiment (see table 2) as well as the probability measured for ^{12}C in a previous experiment [22]. In the case of ^{27}Al the measured value is comparable with calculations of both Coupat et al. and Troitskii et al.. Troitskii et al. give a probability $\leq 10^{-3}$ of single-nucleon absorption of slow pions by finite medium and heavy nuclei, and estimate an enhancement of such a probability by $>10^{2}$ times if a pion condensate exists in the nucleus.

The single-proton emission was measurable only for ^{16}O where a yield of 10^{-3} was obtained. Calculations of ref.6 give for ^{12}C a yield of the order of 10^{-4}.

From the inclusive neutron and proton spectra for E_n, $E_p \geq 20$ MeV, shown in figs.6-12 it is not easy to extract definite information about the pion absorption mechanism, that is, the competition between two- and multi-nucleon mechanisms as well as the effects of final state interactions.

However, in the neutron spectrum of ^6Li the contribution of the direct processes (π^-,nn) and (π^-,np) emitting neutrons and protons around 65 MeV is evident. For the other nuclei the contribution from these two channels is implied by the fact that the spectra extend up to energies which are consistent with the kinematical limits of such reactions.

On the other hand, calculations of Chiang and Hüfner [3] for ^{12}C, based on the two-nucleon mechanism, reasonably reproduce both the neutron and proton spectra for ^{16}O above 60 MeV, whereas, calculations of Jackson and Brenner [4] for ^{16}O, based on the α-cluster mechanism, give much softer neutron and proton spectra than those of the present experiment, ending at about 90-100 MeV and 70-80 MeV, respectively. It is then reasonable to conclude that the high energy part of the neutron and proton spectra is dominated by the two-nucleon absorption reaction. This conclusion is also supported by the fact that the experimental ratios R_{np} (table 4) are consistent with the ratio calculated by Chiang and Hüfner for ^{12}C. Notice that the ratio R of the matrix elements for pion absorption by a np or a pp pair (table 4) results to be independent of the studied nucleus.

Finally, on the basis of the agreement between the measured ratios R_{np} and the results of the microscopic calculations of Shimizu and Faessler [25] one can conclude that the two-nucleon absorption model without rescattering cannot reproduce the experimental ratios.

From the results of this experiment it turned out that the neutron spectra are higher in magnitude than the proton spectra by a factor of ~10. In the framework of the two-nucleon absorption model, the primary neutrons contributing to the neutron spectra originate from pion absorption on both (n,p) and (p,p) pairs whereas the proton spectra are fed by absorptions on (p,p) pairs only. The factor of ~10 cannot be justified solely on the basis of the statistical ratio of (n,p) to (p,p) pairs in the absorbing nucleus and a natural explanation could be given in terms of suppression of pion absorption by T = 1 nucleon pairs [30].

The emission of complex charged particles is also barely understood. Calculations of deuteron spectra [7,8] based on the two-nucleon and pickup mechanism reasonably reproduce the experiments, as shown for ^{16}O. But the cluster-absorption could also justify some spectral features, as discussed in the case of ^{6}Li. In this regard, the statement that deuterons have no chance to get out of the target nucleus, because of their too short mean free path compared to nuclear dimensions [7], cannot be applied to light nuclei, that is, nuclei having radii comparable with the deuteron mean free path, such as ^{6}Li. Moreover, it has to be noticed that the mean free path concept has not a straightforward definition in the case of light nuclei, and anyhow, where such concept is applicable, it is accompanied by different values. Thus, in the case of light nuclei the knock-out of complex charged particles pre-existing in the nuclear structure should also be taken into account.

We wish to acknowledge the cooperation of the members of the cyclotron crew of TRIUMF. We also express our gratitude for the generous hospitality of TRIUMF and the continuous help that we have received during our stay in Vancouver. Finally, we want to thank Mr. G. Milani and G. Becciani for their essential technical assistence during the assemblage of the experimental apparatus.

REFERENCES

1. D.S.Koltun, Adv. Nucl. Phys. 3(1969)71; J.Hüfner, Phys. Rev. C21(1975)1

2. V.S.Buttsev, A.S.Iljinov and S.E.Chigrinov, Sov. J. Part. Nucl. 11(1980)358

3. H.C.Chiang and J.Hüfner, Nucl. Phys. A352(1981)442

4. D.F.Jackson and D.J.Brenner, Progress in Particle and Nuclear Physics, ed. D.Wilkinson (Pergamon, Oxford, 1981), vol. 5 p. 143

5. J.Letourneaux and J.M.Eisenberg, Nucl. Phys. 87(1966)331

6. B.Coupat, P.Bertin and D.Issabelle, Nucl. Phys. A403(1983)497

7. F.Hachenberg, H.C.Chiang and J.Hüfner, Phys. Lett. 97B(1980)183

8. V.M.Datar and B.K.Jain, Phys. Rev. C26(1982)616

9. B.Bassalleck, H.D.Engelhardt, W.D.Klotz, T.Takeutchi, H.Ullrich and M.Furic, Nucl. Phys. A319(1979)397

10. U.Klein, G.Buche, W.Kluge, H.Matthay, G.Mechtersheimer and A.Moline, Nucl. Phys. A329(1979)339

11. R.Madey, T.Vilaithong, B.D.Anderson, J.N.Knudson, T.R.Witten, A.R.Baldwin and F.M.Waterman, Phys. Rev. C25(1982)3050

12. H.P.Isaak, P.Heusi, H.S.Pruys, R.Engfer, E.A.Hermes, T.Kozlowski, U.Sennhauser and H.K.Walter, Helv. Phys. Acta 55(1982)477

13. U.Sennhauser, H.J.Pfeiffer, H.K.Walter, F.W.Schleputz, H.S.Pruys, R.Engfer, R.Hartmann, E.A.Hermes, P.Heusi, H.P.Isaak and W.H.A.Hesselink, Nucl. Phys. A386(1982)429

14. C.Cernigoi, R.Cherubini, N.Grion, G.Pauli and R.Rui, Report INFN/AE - 82/9

15. C.J.Oram, J.B.Warren, G.H.Marshall and J.Doornbos, Nucl. Instr. and Meth. 179(1981)95

16. R.L.Crawn, Nucl. Instr. and Meth. 80(1970)239

17. C.Cernigoi, N.Grion and G.Pauli, Nucl. Instr. and Meth. 131(1975)495

18. C.Cernigoi, N.Grion, G.Pauli and B.Saitta, Nucl. Instr. and Meth. 144(1977)479

19. C.Cernigoi, N.Grion, G.Pauli and B.Saitta, Nucl. Instr. and Meth. 165(1979)401

20. N.R.Stanton, Report COO-1545-92(1971), Ohio State University

21. C.Cernigoi, I.Gabrielli, N.Grion, G.Pauli, B.Saitta, R.A.Ricci, P.Boccaccio and G.Viesti, Nucl. Phys. A352(1981)343

22. C.Cernigoi, N.Grion, G.Pauli, R.Rui, R.Cherubini and D.R.Gill, Nucl. Phys. A411(1983)382

23. C.Cernigoi, N.Grion, G.Pauli, R.Rui and R.Cherubini, Nucl. Instr. and Meth. 211(1983)129

24. K.Nakayama, E.F.Pessoa and R.A.Douglas, Nucl. Instr. and Meth. 190(1981)555

25. K.Shimizu and A.Faessler, Nucl. Phys. A333(1980)495

26. P.Heusi, H.P.Isaak, H.S. Pruys, R.Engfer, E.A.Hermes, T.Kozlowski, U.Sennhauser and H.K.Walter, Nucl. Phys. A407(1983)429

27. M.P.Guthrie, R.G.Alsmiller,Jr. and H.W.Bertini, Nucl. Instr. and Meth. 66(1968)29

28. F.Hachengerg, Phys. Lett. 113B(1982)451

29. M.A.Troitskii, M.V.Koldaev and N.I.Chekunaev, JETP Lett. 25(1977)123

30. H.Toki and H.Sarafian, Report PHY-80-17605 (Work supported by the National Science Foundation); T.S.H.Lee and K.Ohta, Phys. Rev. Lett. 49(1982)1079

31. R.Hartmann, H.P.Isaak, R.Engfer, E.A.Hermes, H.S.Pruys, W.Dey, H.J.Pfeiffer, U.Sennhauser, H.K.Walter and J.Morgenstern, Nucl. Phys. A308(1978)345

Table 1

Characteristics of targets

Target	Thickness (g/cm^2)	π^--stopped (10^5 π^-/sec)	π^--energy (MeV)	channel	ratio in/out
^{6}Li	0.30	1.64	43	M13	2.17
^{9}Be	0.55	1.83	43	M13	2.42
^{16}O	0.19	1.57	43	M13	2.08
	2.43	0.26	90	M11	6.44
^{27}Al	1.78	0.19	90	M11	4.68

Table 2

Measured rates per 100 stopped pions of the single-neutron emission reaction (π^-,n) in ^{6}Li, ^{9}Be, ^{12}C, ^{16}O and ^{27}Al compared with other results

Reaction	^{6}Li	^{9}Be	^{12}C	^{16}O	^{27}Al	Reference
(π^-,n)	1.31±0.29	2.46±0.40	1.70±0.34	1.25±0.27	0.32±0.11	this work a)
	0.16±0.08	< 0.15	0.10±0.05			[9]

a) The value for ^{12}C is taken from ref. 22.

Table 3

Measured multiplicities $\bar{\nu}$ of neutrons, protons and deuterons from absorption of stopped negative pions in ^{6}Li, ^{9}Be, ^{12}C, ^{16}O and ^{27}Al compared with other results

	^{6}Li	^{9}Be	^{12}C	^{16}O	^{27}Al	Reference	
$\bar{\nu}_n[n/\pi^-]$	1.98±0.21	2.12±0.22	1.25±0.11	1.72±0.18	1.50±0.16	this work	a)
	1.55±0.23		1.21±0.18			[12]	b)
			1.6±0.3	1.7±0.3		[10]	c)
			1.77±0.15	1.78±0.16	1.67±0.23	[11]	c)
			1.45±0.10			[31]	c)
$\bar{\nu}_p\left[(p/\pi^-)\times 10^2\right]$	11.3±0.7	9.1±0.6	9.4±0.6	14.4±0.9		this work	a)
	10.7±1.6					[13]	d)
$\bar{\nu}_d\left[(d/\pi^-)\times 10^2\right]$	5.5±0.3	4.8±0.3		3.8±0.2		this work	a)
	4.2±0.6					[13]	e)

a) The off-line thresholds were 18, 24 and 30 MeV for n, p and d respectively. Data on ^{12}C are taken from ref. 22.
b) Multiplicity for $E_n > 20$ MeV
c) Multiplicity of direct neutrons (total spectrum minus evaporation neutrons)
d) Multiplicity of protons in the energy interval 20-70 MeV
e) Multiplicity of deuterons in the energy interval 40-70 MeV

Table 4

Ratio R_{np} describing the relative importance of nn to np emission; ratio R of the matrix elements for pion absorption by a np or a pp pair; ratio R_{stat} expressing the relative probability to find a np or pp pair in the nucleus.

Ratio	^{6}Li	^{9}Be	^{16}O
$\frac{\bar{\nu}_n}{\bar{\nu}_p}$	18.0±3.0	25.4±4.3	15.5±2.5
R_{np}	8.5±1.6	12.2±2.3	7.3±1.3
$R_{stat} = \frac{2N}{Z-1}$	3.0	3.3	2.3
R	2.8±0.6	3.7±0.7	3.2±0.5

Neutron and proton yields ν_n and ν_p were selected in the same high energy region ($E_{n,p} \geq 96$ MeV) from the n and p inclusive energy spectra respectively. n and p events due to four body final state (X+3N) channels were rejected by cutting n and p spectra over the X+3N kinematical limit. Single n and p emission contributions were dropped by three body phase space calculations.

Figure captions

1. Experimental set-up.

2. Range curve for ^{16}O target.

3. Energy (solid curve) and relative yield (dashed curve) of muons from 12-MeV pion decays as a function of angle in the laboratory system.

4. TOF spectrum (background subtracted) of neutrons emitted following the absorption of stopped negative pions in ^{6}Li.

5. High-energy part of the TOF spectrum of neutrons emitted following the absorption of stopped negative pions in ^{6}Li with background subtracted.

6. Inclusive energy spectrum of neutrons emitted after stopped negative pion absorption in ^{6}Li. Chance coincidence background is indicated by the dashed line. The solid line represents a phase-space calculation for the two-neutron emission reaction $^{6}Li(\pi^-,2n)^{4}He$. The spectra measured by Bassalleck et al. [9] (histogram) and by Isaak et al. [12] (open triangles) are shown for comparison.

7. Inclusive energy spectrum of neutrons emitted after stopped negative pion absorption in ^{9}Be. Chance coincidence background is indicated by the dashed line. The solid line represents a phase-space calculation for the two-neutron emission reaction $^{9}Be(\pi^-,2n)^{7}Li$.

8. Inclusive energy spectrum of neutrons emitted after stopped negative pion absorption in ^{16}O. Chance coincidence background is indicated by the dashed line. The solid line represents a phase-space calculation for the two-nucleon emission reaction $^{16}O(\pi^-,np)^{14}C$. The bell curve (full line, log scale) represents the contribution to the spectrum due to the single-neutron emission reaction $^{16}O(\pi^-,n)^{15}N$. The spectrum measured by Madey et al. [11] (open triangles) is shown for comparison. The dashed-dotted curve represents a calculation of Chiang and Hüfner [3] for ^{12}C, and the dotted curve a calculation of Jackson and Brenner [4] for ^{16}O.

9. Inclusive energy spectrum of neutrons emitted after stopped negative pion absorption in ^{27}Al. Chance coincidence background is indicated by the dashed line. The solid line represents a phase-space calculation for the two-neutron emission reaction $^{27}Al(\pi^-,2n)^{25}Mg$. The spectrum measured by Madey et al. [11] (open triangles)

is shown for comparison.

10. Inclusive energy spectra of protons and deuterons emitted after stopped negative pion absorption in ^{6}Li. The spectra of protons (open circles) and deuterons (open squares) measured by Sennhauser et al. [13] are shown for comparison.

11. Inclusive energy spectra of protons and deuterons emitted after stopped negative pion absorption in ^{9}Be.

12. Inclusive energy spectra of protons and deuterons emitted after stopped negative pion absorption in ^{16}O. Chance coincidence background is indicated by the dotted-dashed line. The solid line (b) represents a phase-space calculation for the two-nucleon emission reaction $^{16}O(\pi^-,np)^{14}C$. The solid curve (a) represents the proton spectrum calculated for ^{12}C by Chiang and Hüfner [3]. The dashed curve represents the deuteron spectrum calculated for ^{12}C by Datar and Jain [8].

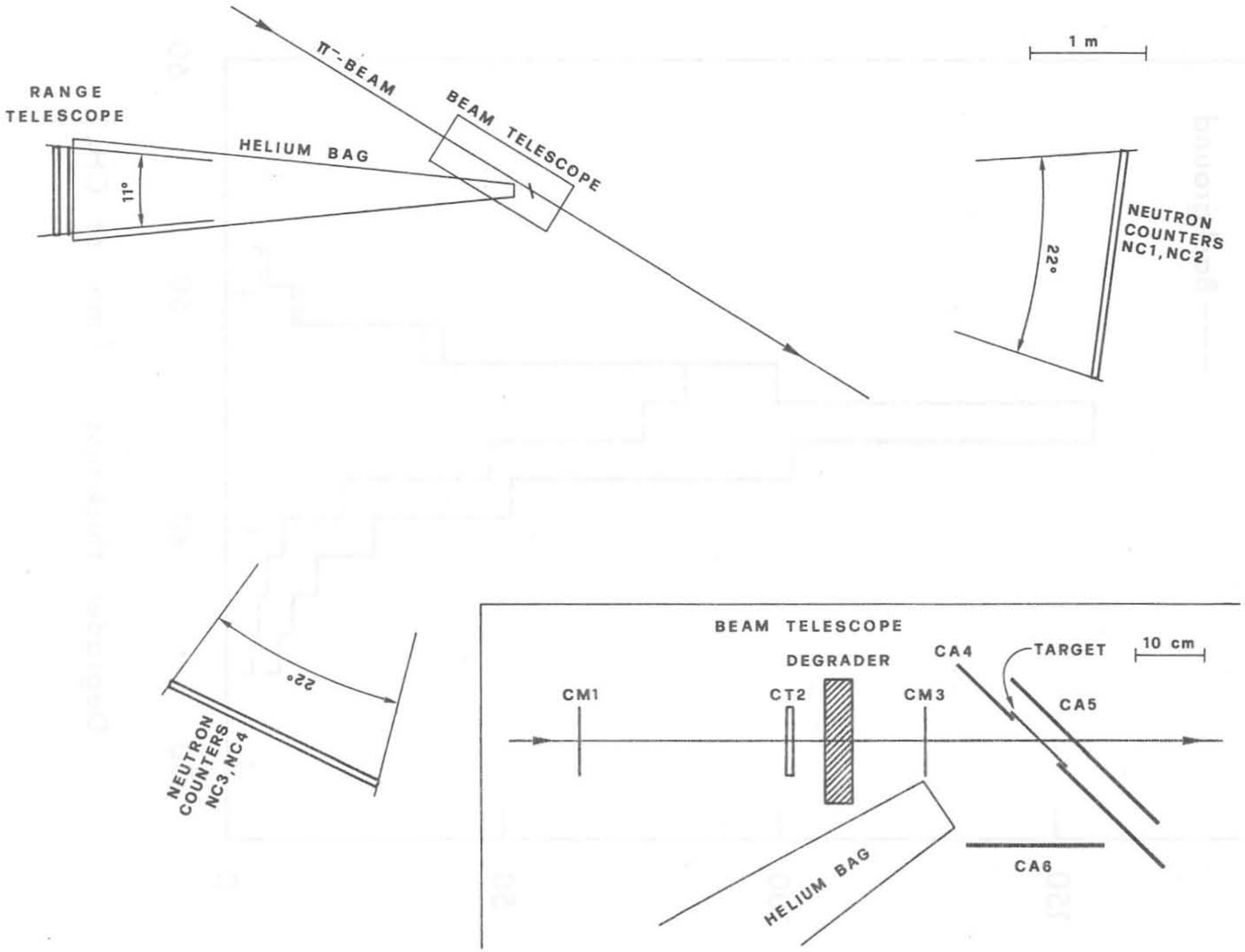
RANGE TELESCOPE
HELIUM BAG
11°
π⁻-BEAM
BEAM TELESCOPE
1 m
NEUTRON COUNTERS NC1, NC2
22°
NEUTRON COUNTERS NC3, NC4
22°
BEAM TELESCOPE
DEGRADER
CA4
TARGET
10 cm
CM1
CT2
CM3
CA5
CA6
HELIUM BAG

FIG. 1

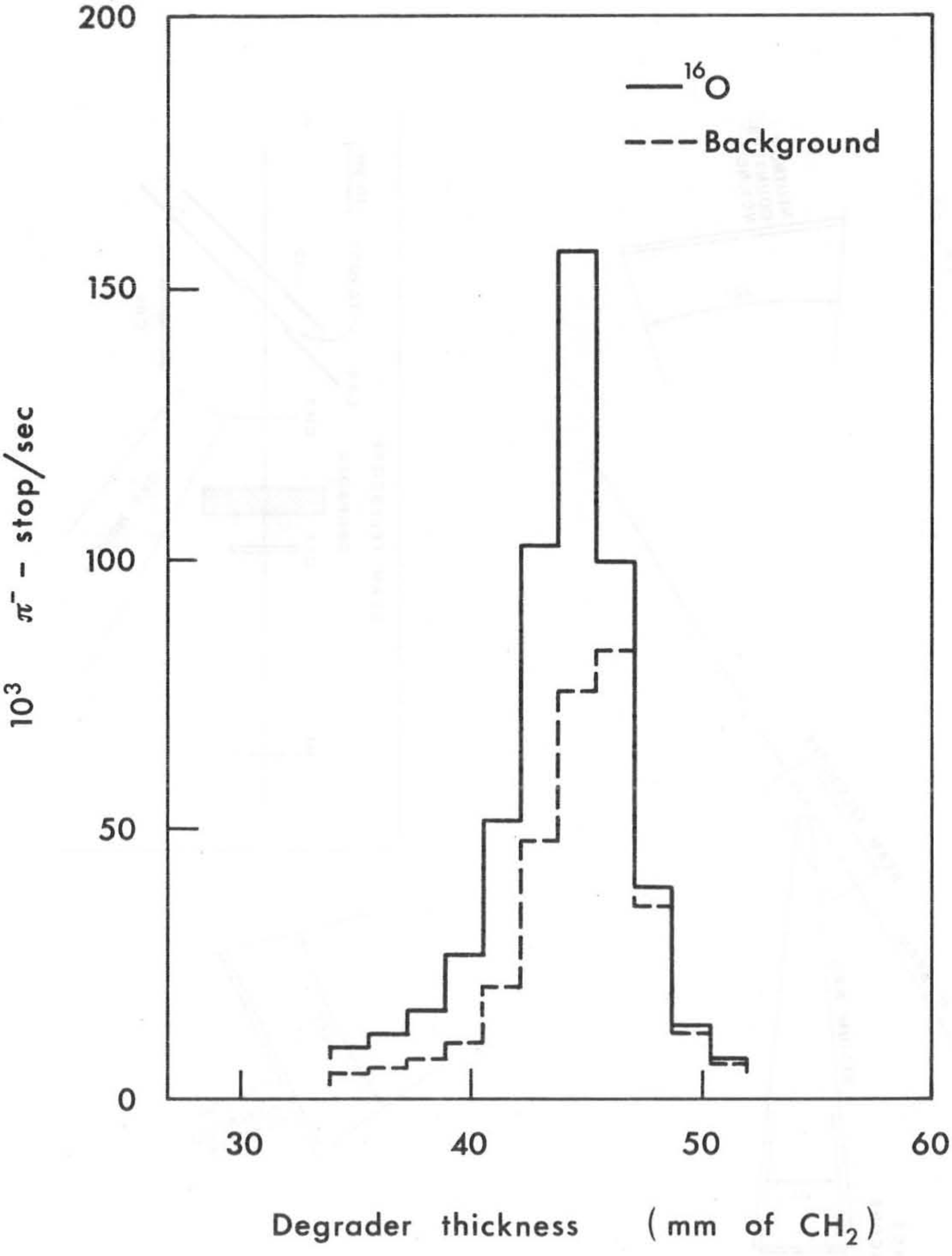
200
150
100
50
0
—^{16}O
- - - Background
10^3 π^- - stop/sec
30
40
50
60
Degrader thickness (mm of CH_2)

FIG. 2

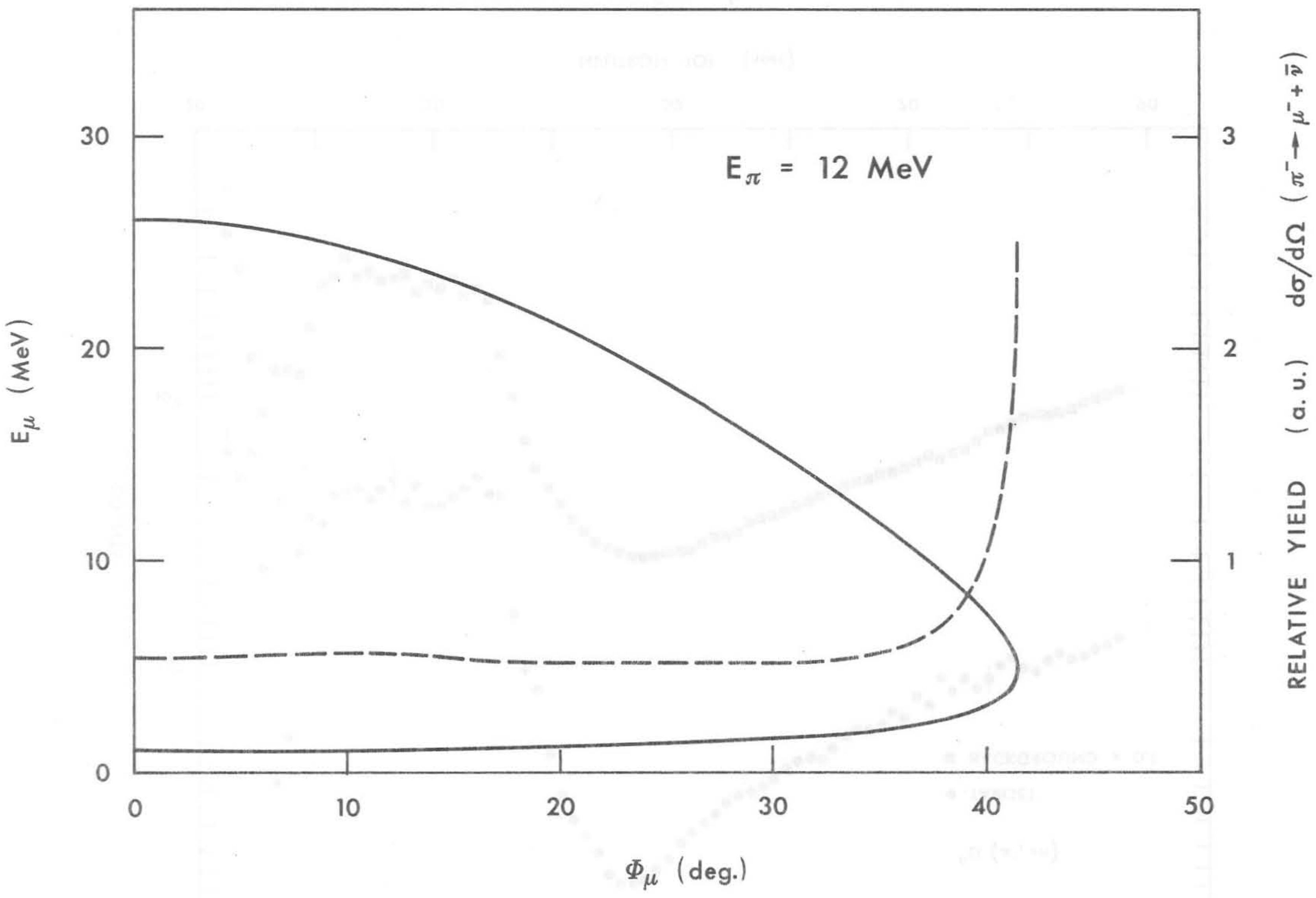

E_π = 12 MeV
E_μ (MeV)
30
20
10
0
0
10
20
30
40
50
Φ_μ (deg.)
3
2
1
RELATIVE YIELD (a. u.) $d\sigma/d\Omega$ $(\pi^- \to \mu^- + \bar{\nu})$

FIG. 3

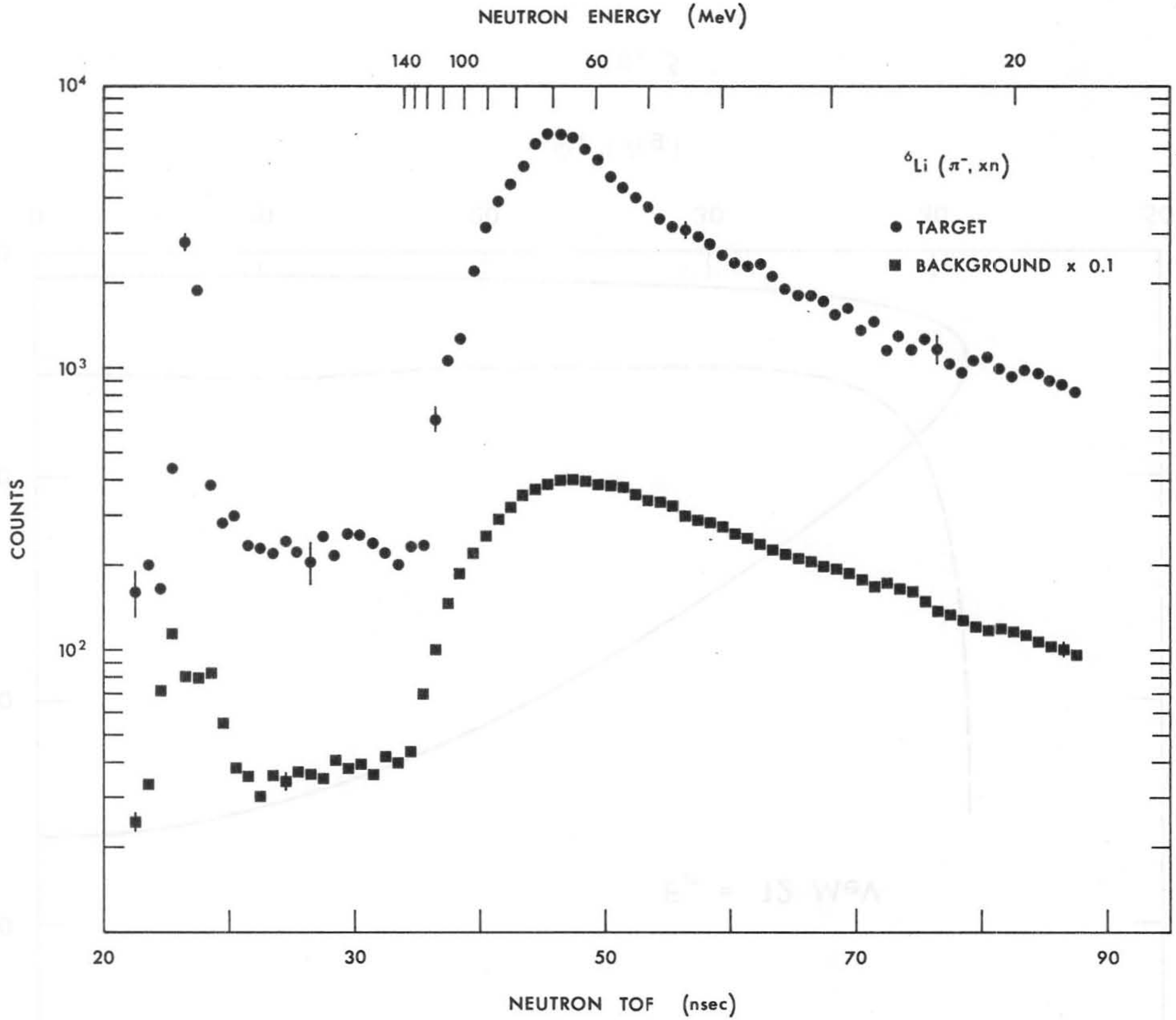
NEUTRON ENERGY (MeV)
140
100
60
20
10^4
10^3
10^2
COUNTS
^{6}Li (π^-, xn)
● TARGET
■ BACKGROUND x 0.1
20
30
50
70
90
NEUTRON TOF (nsec)

FIG. 4

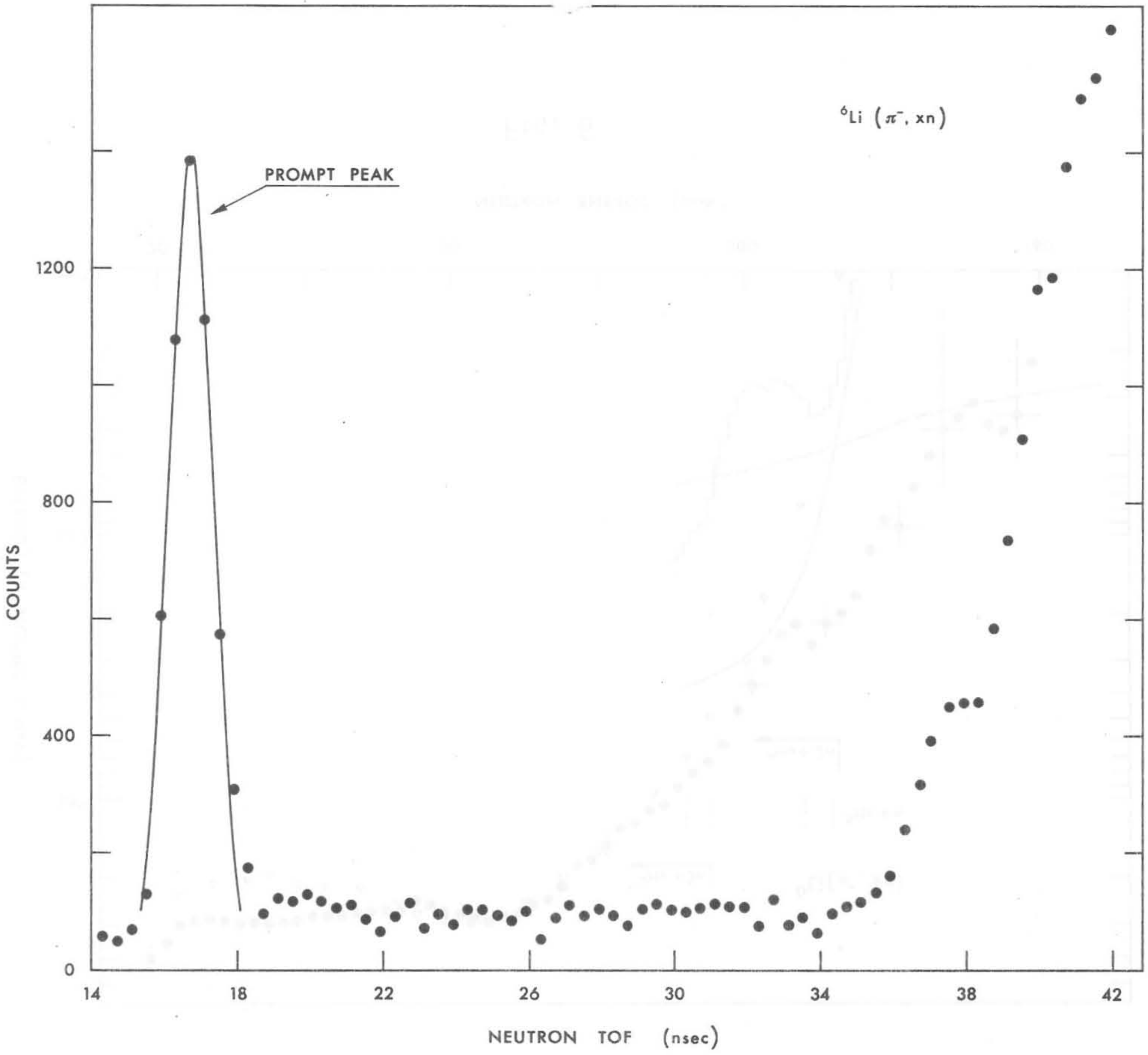

^6Li (π^-, xn)
PROMPT PEAK
COUNTS
0
400
800
1200
14
18
22
26
30
34
38
42
NEUTRON TOF (nsec)

FIG. 5

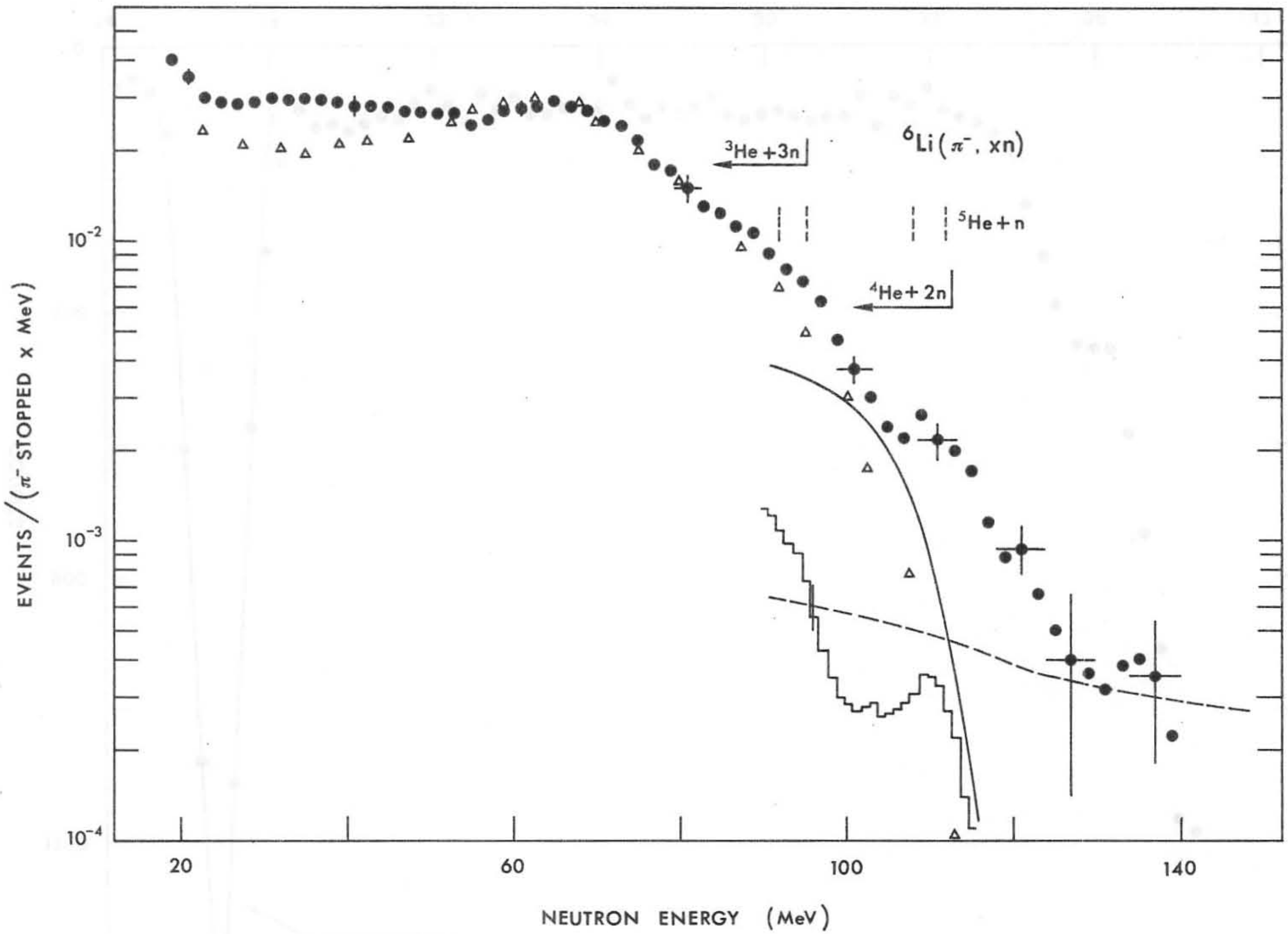

$^6Li(\pi^-, xn)$
$^3He+3n$
^5He+n
$^4He+2n$
10^{-2}
10^{-3}
10^{-4}
20
60
100
140
EVENTS / (π^- STOPPED x MeV)
NEUTRON ENERGY (MeV)

FIG. 6

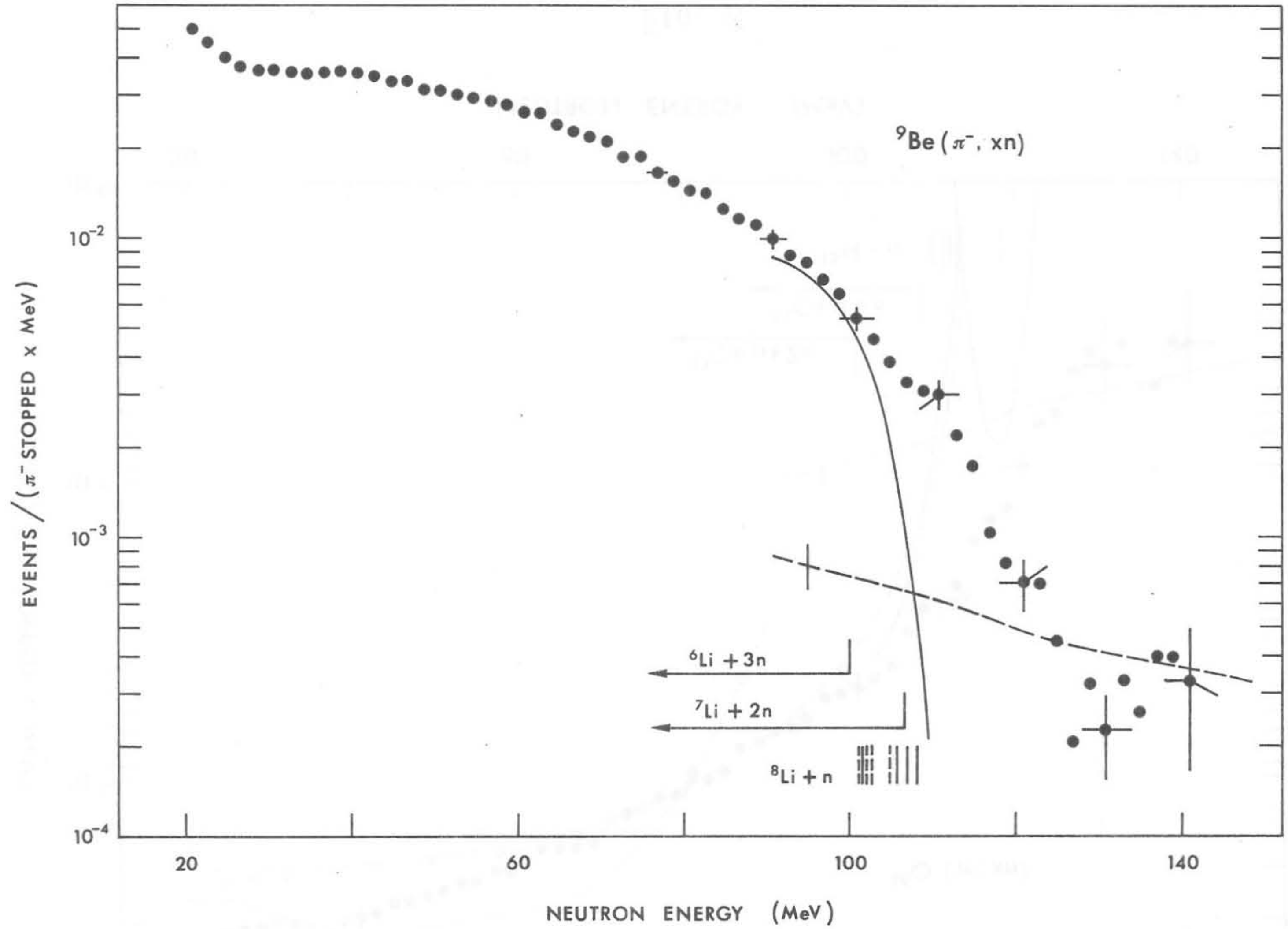
^{9}Be (π^-, xn)
EVENTS / (π^- STOPPED x MeV)
10^{-2}
10^{-3}
10^{-4}
^{6}Li + 3n
^{7}Li + 2n
^{8}Li + n
20
60
100
140
NEUTRON ENERGY (MeV)

FIG. 7

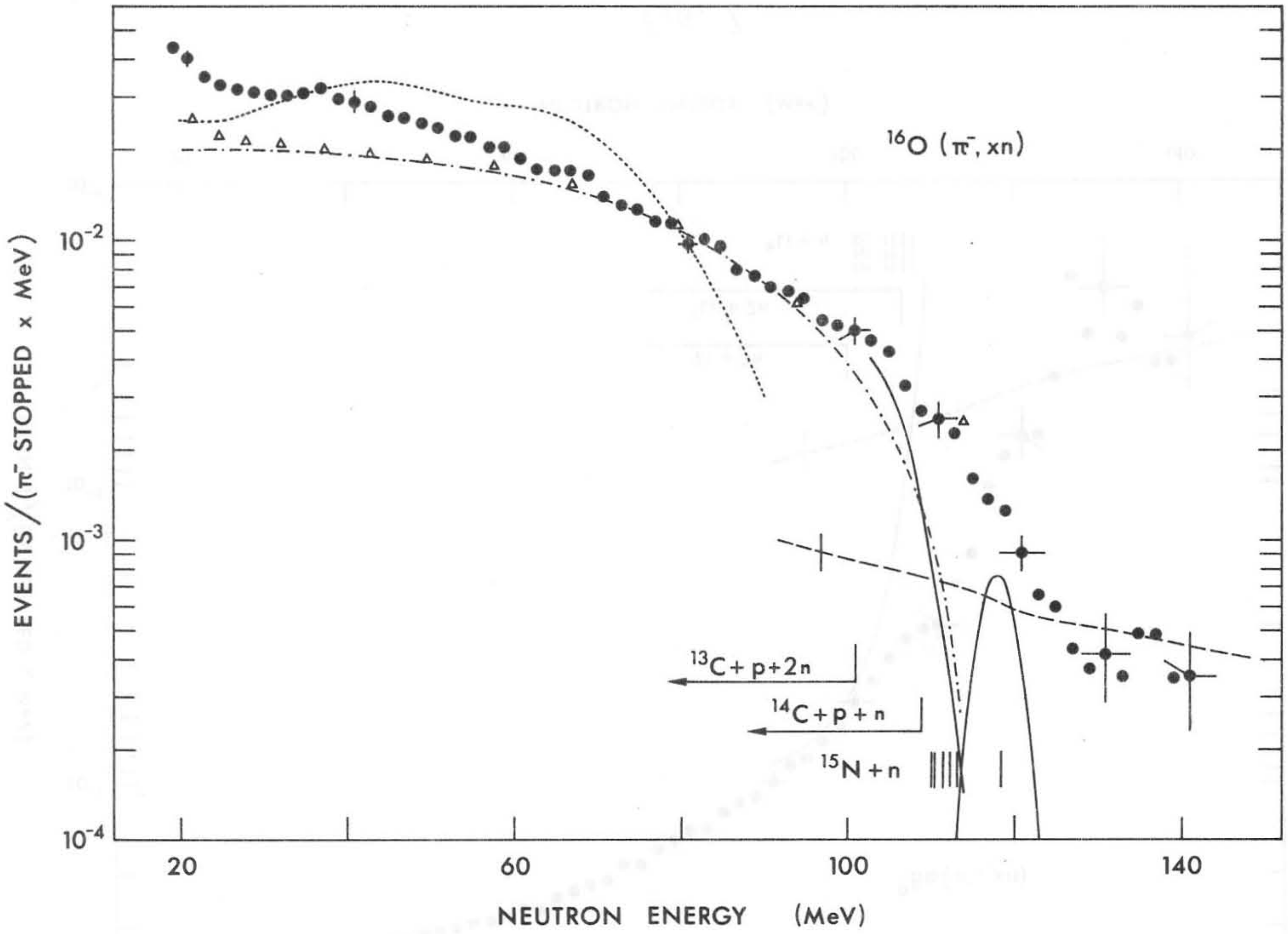

^{16}O (π^-, xn)
10^{-2}
10^{-3}
10^{-4}
EVENTS / (π^- STOPPED x MeV)
^{13}C + p + 2n
^{14}C + p + n
^{15}N + n
20
60
100
140
NEUTRON ENERGY (MeV)

FIG. 8

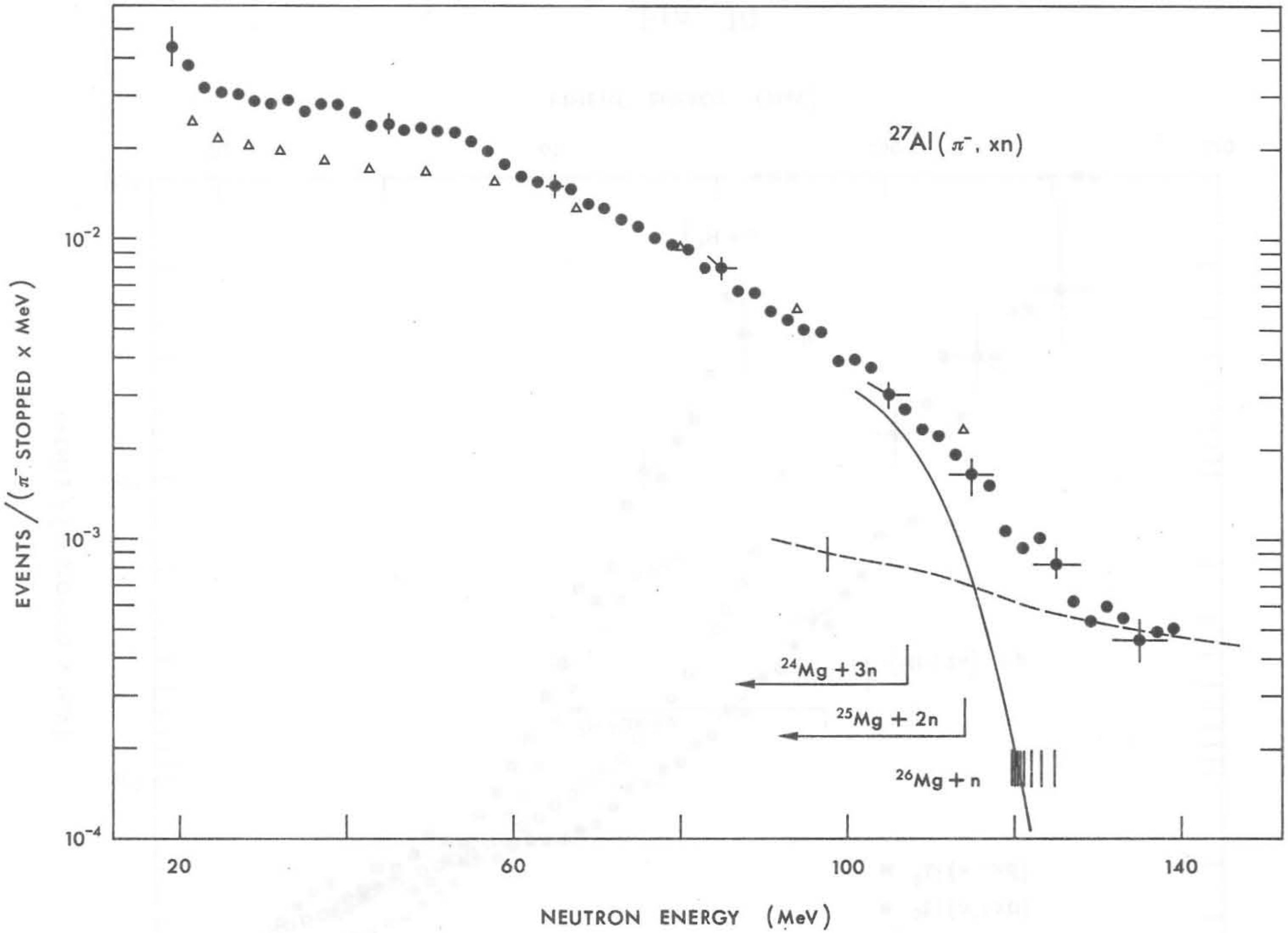
^{27}Al(π^-, xn)
EVENTS / (π^- STOPPED x MeV)
10^{-2}
10^{-3}
10^{-4}
20
60
100
140
NEUTRON ENERGY (MeV)
^{24}Mg + 3n
^{25}Mg + 2n
^{26}Mg + n

FIG. 9

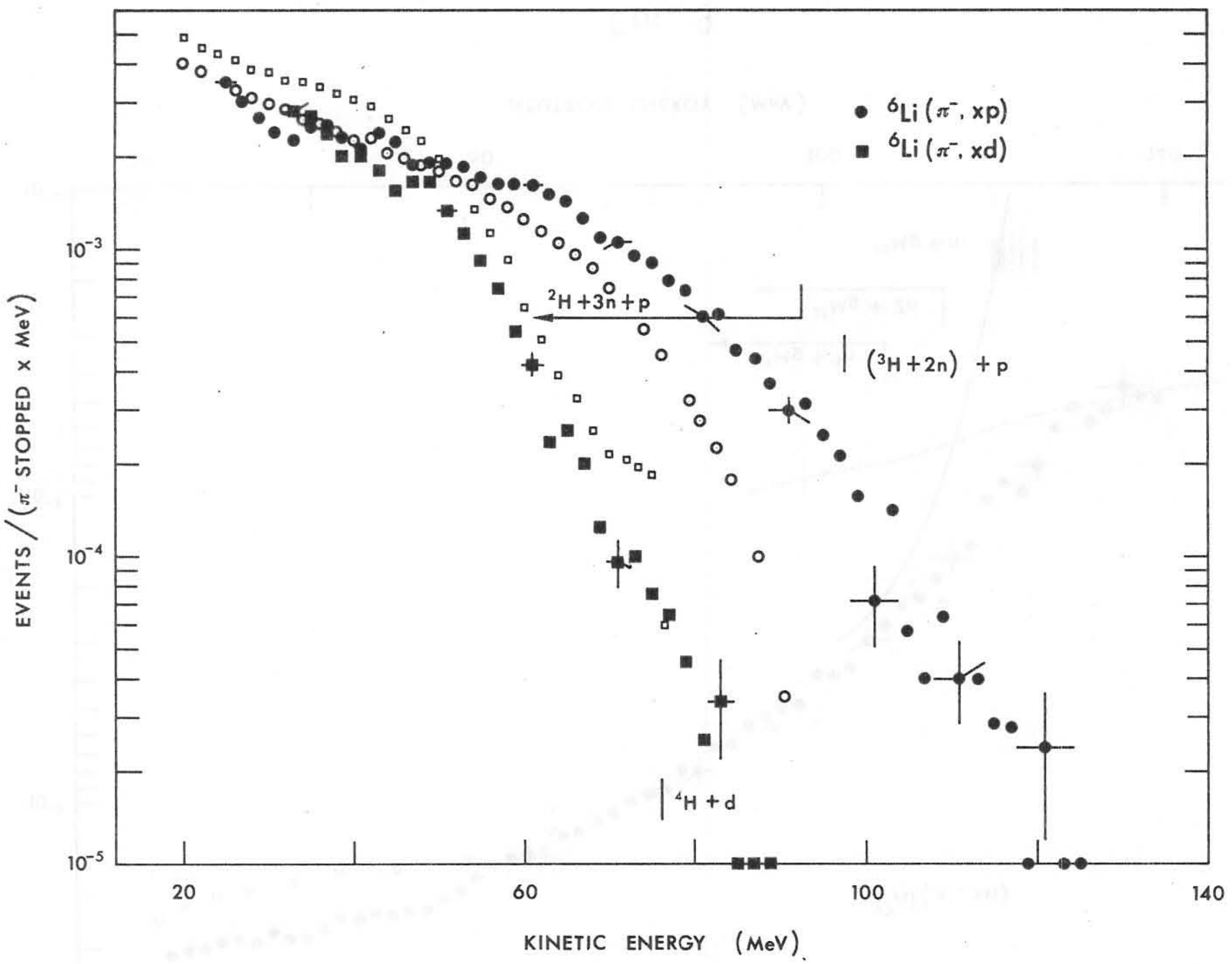

$^6Li(\pi^-, xp)$
$^6Li(\pi^-, xd)$
$^2H+3n+p$
$(^3H+2n)+p$
^4H+d
10^{-3}
10^{-4}
10^{-5}
EVENTS / (π^- STOPPED x MeV)
20
60
100
140
KINETIC ENERGY (MeV)

FIG. 10

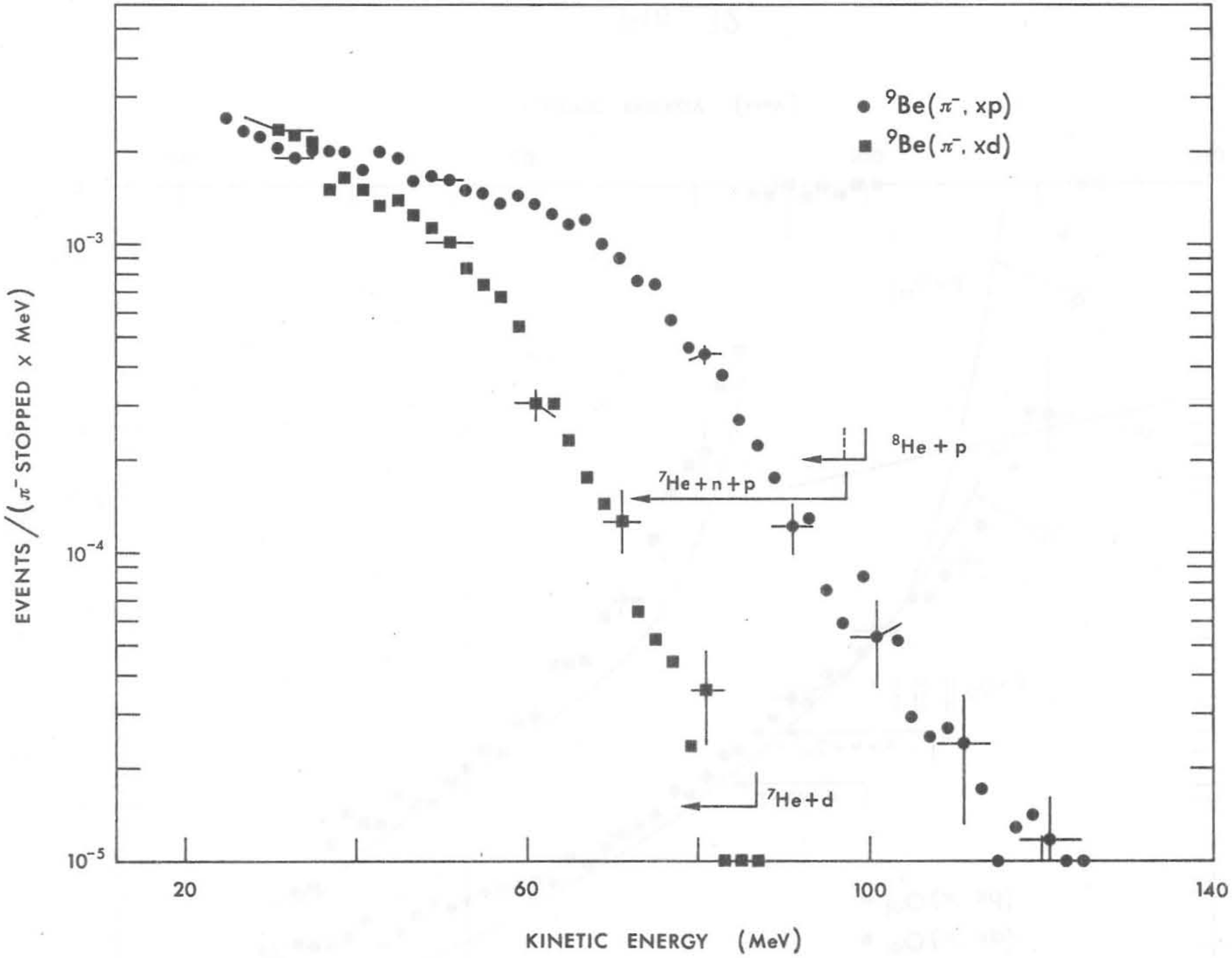

$^9Be(\pi^-, xp)$
$^9Be(\pi^-, xd)$
$^8He + p$
$^7He + n + p$
$^7He + d$
10^{-3}
10^{-4}
10^{-5}
20
60
100
140
EVENTS / (π^- STOPPED x MeV)
KINETIC ENERGY (MeV)

FIG. 11

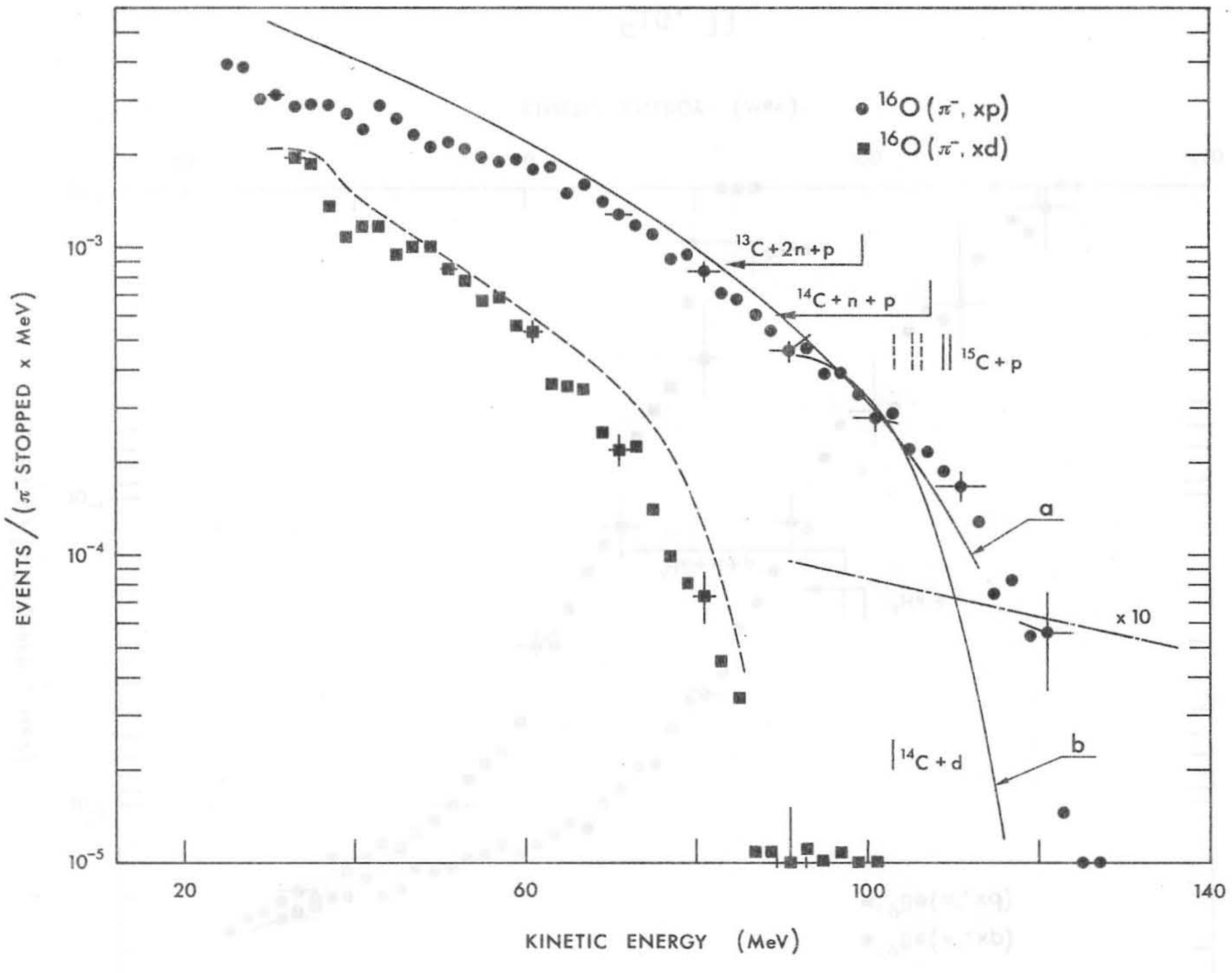

$^{16}O(\pi^-, xp)$
$^{16}O(\pi^-, xd)$
$^{13}C+2n+p$
$^{14}C+n+p$
$^{15}C+p$
$^{14}C+d$
a
b
x 10
10^{-3}
10^{-4}
10^{-5}
20
60
100
140
EVENTS / (π^- STOPPED x MeV)
KINETIC ENERGY (MeV)

FIG. 12